Optics Communications 285 (2012) 3264–3268

Contents lists available at SciVerse ScienceDirect

Optics Communications

journal homepage: www.elsevier.com/locate/optcom

Optical delay with spectral hole burning in Doppler-broadened cesium vapor

Monte D. Anderson [a,*], Glen P. Perram [b]

[a] Department of Physics, United States Air Force Academy, 2354 Fairchild Drive, U.S. Air Force Academy CO 80840, United States
[b] Department of Engineering Physics, Air Force Institute of Technology, 2950 Hobson Way, Wright-Patterson Air Force Base OH 45433, United States

ARTICLE INFO

Article history:
Received 22 January 2012
Accepted 26 March 2012
Available online 9 April 2012

Keywords:
Hole burning
Slow light
Group delay
Alkali metal vapor

ABSTRACT

The full frequency dependence of the optical delay in the Cs D_1 ($6\,^2S_{1/2}-6\,^2P_{1/2}$) line has been observed, including all four hyperfine split components. Pulse delays of 1.6 ns to 24.1 ns are obtained by scanning across the hyperfine splitting associated with the lower $^2S_{1/2}$ state. Optical control of pulse delays in cesium vapor was demonstrated by pumping the D_2 ($6\,^2S_{1/2}-6\,^2P_{3/2}$) transition and observing resulting holes in the D_1 delay spectrum. For a pump at four times the saturation intensity, the pulse delays are reduced by a maximum of 78% in a narrow region of 110 MHz. The frequency dependence of the delays of the probe laser in the vicinity of the spectral holes agrees with a Kramers–Kronig model prediction.

Published by Elsevier B.V.

1. Introduction

Numerous applications from communications to interferometry for remote sensing stand to benefit from the tunable delay of optical pulses. Several methods seek to achieve a rapidly tunable optical delays of multiple pulse widths with minimal loss of signal amplitude and no pulse dispersion. Coherently coupled fields can produce slow light through electromagnetically induced transparency (EIT) [1–3]. Alternatively pulse delays may be controlled by scanning through the rapidly varying frequency-dependent absorption near atomic transitions [4–7]. We previously reported controlling optical delay by tuning a single laser across the D_2 ($6\,^2S_{1/2}-6\,^2P_{3/2}$) absorption spectrum of cesium vapor [7]. By extending the spectral analysis to include Voigt profiles with the Doppler component, the full frequency dependence of the observed delays was adequately described. In this paper we extend the analysis to the Cs D_1 ($6\,^2S_{1/2}-6^2P_{1/2}$) spectrum where the hyperfine splitting is large enough to resolve all four components.

Agarwal and Dey proposed producing pulse delays with hole burning in a Doppler-broadened atomic vapor using a counter propagating pump beam to saturate the media and achieve group indices of about 10^3 [8]. Narrower resonances may be achieved using quantum coherence effects [9]. Shakhmuratov et al. extended the technique to persistent spectral hole burning and slow light in inhomogeneously broadened solid materials [10]. Most recently, Camacho et al. experimentally realized these concepts in hot rubidium vapor [11]. The pump laser induces transparency by moving population from the probed hyperfine state to the other hyperfine component, not by coherent effects. This previous work focused on frequency modulation of the pump beam to tune delays of up to 45 ns [11].

In the current experiment we use a continuous wave (cw) D_2 pump laser to depopulate a given velocity group in the Cs ground state and probe the full frequency dependence of the delays observed in the D_1 absorption spectrum. Monitoring pulse delays as a function of probe frequency clearly revealed a pump intensity dependent hole.

2. Experimental setup

The experimental apparatus for hole burning delay measurements shown in Fig. 1 is a modified sub-Doppler absorption spectroscopy experiment where counter propagating beams intersect in the hot cesium vapor cell. A New Focus Velocity™ model 6316 20-mW tunable diode laser with a linewidth less than 300 kHz serves as the pump laser on the D_2 Cs transition (852 nm). The pump laser is directed through a pellicle beam splitter where a beam sample is sent to a Bristol model 621A wavelength meter with 0.075 GHz (0.0025 cm^{-1}) accuracy for frequency reference. The main pump beam is directed through a 5-cm-long, low-pressure cesium vapor cell enclosed in a machined aluminum heater block maintained at a constant temperature of ± 2 °C between 40 °C and 120 °C. Pump power is adjusted using neutral density filters as changing diode current causes a subsequent shift in pump laser frequency.

A New Focus Velocity™ model 6318 6-mW tunable diode laser with less than 300-kHz linewidth is used as the D_1 probe laser at 894 nm. The probe beam is directed through an optical isolator and a pellicle beam splitter. A probe beam sample is sent to a second Bristol model 621A wavelength meter while the main probe beam continues to a EOSPACE fiber-coupled Mach–Zehnder interferometric lithium niobate ($LiNbO_3$) electro-optic intensity modulator (EOM). A Picosecond Pulse Labs 1.6-GHz pulse/pattern generator drives the EOM to create a Gaussian 7.5-ns full-width at half-maximum (FWHM) pulse with 133-Hz repetition rate.

* Corresponding author.
E-mail addresses: monte.anderson@usafa.edu (M.D. Anderson), glen.perram@afit.edu (G.P. Perram).

0030-4018/$ – see front matter. Published by Elsevier B.V.
doi:10.1016/j.optcom.2012.03.021

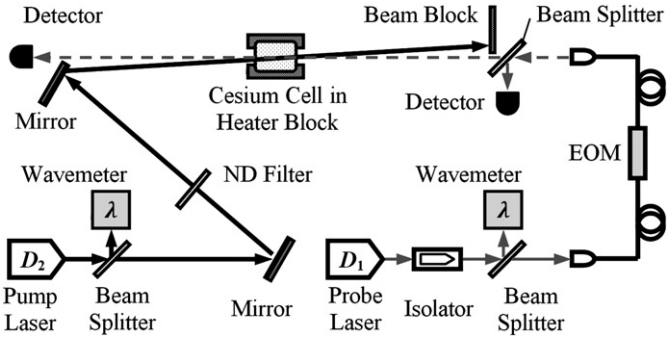

Fig. 1. Experimental setup for hole burning delay measurements.

The modulated probe is split exiting the EOM fiber to a silicon photodiode detector with 2.3-ns response time providing initial intensity reference before the alkali-metal vapor cell. The probe beam is aligned overlapping but counter propagating to the pump beam in the Cs cell enclosed in the heater block. Probe pulse delay is measured after the alkali-metal vapor cell by a silicon photodiode detector with a 1-ns response time.

Pulse delay temporal waveforms of 2000 pulse averages were recorded on a 3-GHz oscilloscope triggered by the pulse generator signal. The cw D_2 pump is set at a fixed power and frequency detuned from an absorption peak. Neutral density filters were placed in the D_2 pump beam path to vary pump power at 0 mW (blocked), 5 mW and 16 mW. The probe laser is scanned across the full D_1 absorption spectrum. For the hole burning experiment the probe laser was scanned with greater sampling near $F''=4$ to $F'=3$ or 4 components as depicted on the Cs energy level diagram in Fig. 2. Simulated absorption coefficients for Cs D_1 and D_2 at 50 °C are shown in Fig. 3. The *x*-axis is labeled using both nanometer (nm) and detuning frequency $\nu_{\Delta 1}$ and $\nu_{\Delta 2}$ (GHz) scales. The frequencies $\nu_{\Delta 1}$ and $\nu_{\Delta 2}$ represent detuning from the central atomic transition frequency $\nu_{D_1}=335.116049$ THz and $\nu_{D_2}=351.725718$ THz. The simulation is performed at zero buffer gas pressure and modeled including Doppler broadening. At 50 °C with Doppler width of 393 MHz, the cesium concentration is $\sim 4.6\times 10^{11}$ atoms/cm^3 and the peak D_1 absorption coefficient is quite high, $\alpha\approx 3.5\,\mathrm{cm}^{-1}$ and the absorbance is $A_\lambda=17.3$. At 100 °C the cesium concentration increases by a factor of ~35 [12].

3. Results

3.1. Optical delay and hyperfine structure

The pulse/pattern generator produced a nearly Gaussian 7.5-ns pulse as shown in Fig. 4. Sample pulses at three D_1 detuning frequencies $\nu_{\Delta 1}$ for the cell at $T=109.5$°C are depicted where pulse (1) is farthest

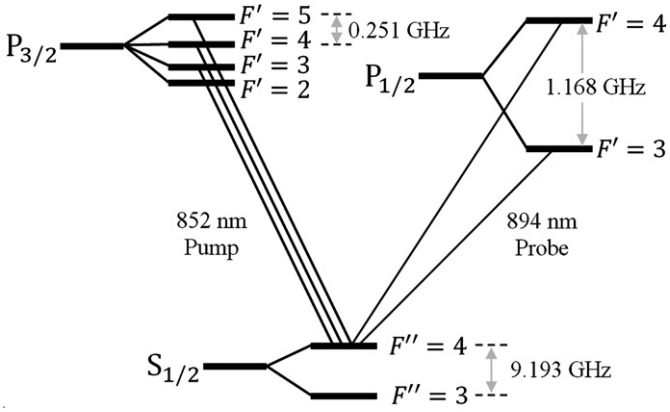

Fig. 2. Energy level diagram depicting the pump D_2 transitions and probe D_1 transitions.

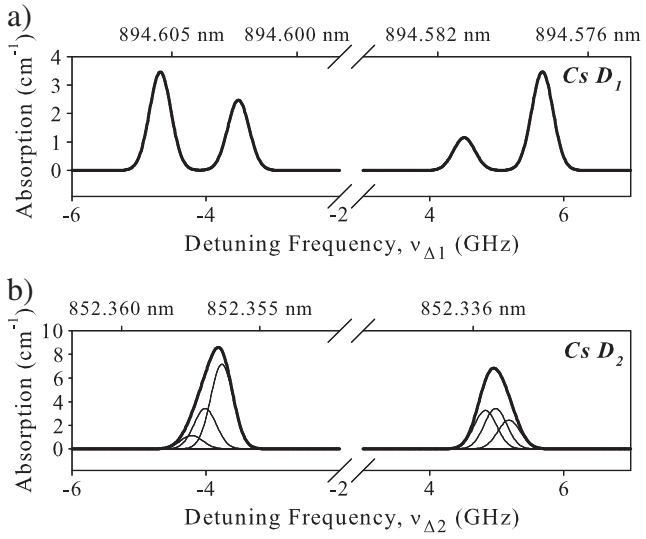

Fig. 3. Simulated absorption coefficients for the (a) D_1 and (b) D_2 transitions at 50 °C. Single hyperfine transition absorption lineshapes are shown in the D_2 spectrum as thin black lines.

from the absorption peak while pulse (3) is closest to the resonant transition frequency. As expected the pulse amplitude decreases for pulses closer to the peak absorption while the pulse width increases due to dispersion broadening. Peak time for each Gaussian fit is recorded as the pulse arrival time. Zero-delay time is determined when the probe is detuned far off resonant frequency and the value is subtracted from the arrival time for each pulse to calculate the pulse delay. Maximum error in delay time measurement is ±0.15 ns with average error ±0.03 ns. Within 2 GHz of the resonant transitions the pulse amplitude is entirely attenuated, and relative delay cannot be determined. The observed delays for the $T=109$ °C cell as a function of prove detuning are illustrated in Fig. 5. Delays of up to 24.1 ns are observed near the two resonant frequencies associated with the ground state hyperfine splitting. However, the absorbance is too high to observe the hyperfine splitting of the upper $^2P_{1/2}$ state. A few "stray" data points are indicated where transmitted pulse intensity is highly attenuated and barely discernible. The present results represent higher frequency sampling with 200 samples over 20 GHz compared to the prior observations for the Cs D_2 line with 90 samples over 20 GHz [7].

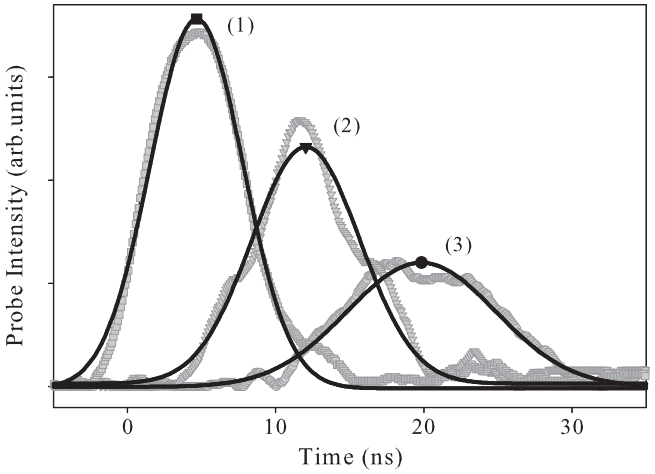

Fig. 4. Transmitted pulses at three D_1 detuning frequencies $\nu_{\Delta 1}$ are depicted as gray shapes. Solid black lines show Gaussian fit curves, and the peak of the fit curve is marked for reference. (1) $\nu_{\Delta 1}=7.44$ GHz, peak at 4.66 ns, width 7.37 ns (2) $\nu_{\Delta 1}=6.73$ GHz, peak at 12.04 ns, width 8.60 ns and (3) $\nu_{\Delta 1}=6.5$ GHz, peak at 19.84 ns, width 11.83 ns.